Supplementary Information

	Experimental ID	Na_2CO_3 [mM]	$CaCl_2{\cdot}2H_2O$ [mM]	Organic additive (OA) [mM]	OA name	OA formula	IAP
1	Exp11_B4	25	5	5	Creatinine	C4H7N3O	125
2	Exp11_B5	25	25	5	Creatinine	C4H7N3O	625
3	Exp11_B6	25	125	5	Creatinine	C4H7N3O	3125
4	Exp11_B7	25	5	25	Creatinine	C4H7N3O	125
5	Exp11_B8	25	25	25	Creatinine	C4H7N3O	625
6	Exp11_B9	25	125	25	Creatinine	C4H7N3O	3125
7	Exp11_E7	25	5	125	Creatinine	C4H7N3O	125
8	Exp11_E8	25	25	125	Creatinine	C4H7N3O	625
9	Exp11_E9	25	125	125	Creatinine	C4H7N3O	3125
10	Exp12_B4	25	5	5	L-asparagine	C4H8N2O3	125
11	Exp12_B5	25	25	5	L-asparagine	C4H8N2O3	625
12	Exp12_B6	25	125	5	L-asparagine	C4H8N2O3	3125
13	Exp12_B7	25	5	25	L-asparagine	C4H8N2O3	125
14	Exp12_B8	25	25	25	L-asparagine	C4H8N2O3	625
15	Exp12_B9	25	125	25	L-asparagine	C4H8N2O3	3125
16	Exp12_E4	25	5	75	L-asparagine	C4H8N2O3	125
17	Exp12_E5	25	25	75	L-asparagine	C4H8N2O3	625
18	Exp12_E6	25	125	75	L-asparagine	C4H8N2O3	3125
19	Exp12_E7	25	5	100	L-asparagine	C4H8N2O3	125
20	Exp12_E8	25	25	100	L-asparagine	C4H8N2O3	625
21	Exp12_E9	25	125	100	L-asparagine	C4H8N2O3	3125
22	Exp13_B4	25	5	5	Trisodium citrate	Na3C6H5O7	125
23	Exp13_B5	25	25	5	Trisodium citrate	Na3C6H5O7	625
24	Exp13_B6	25	125	5	Trisodium citrate	Na3C6H5O7	3125
25	Exp13_B7	25	5	25	Trisodium citrate	Na3C6H5O7	125
26	Exp13_B8	25	25	25	Trisodium citrate	Na3C6H5O7	625
27	Exp13_B9	25	125	25	Trisodium citrate	Na3C6H5O7	3125
28	Exp13_C4	25	5	125	Trisodium citrate	Na3C6H5O7	125
29	Exp13_C5	25	25	125	Trisodium citrate	Na3C6H5O7	625

30	Exp13_C6	25	125	125	Trisodium citrate	Na3C6H5O7	3125
31	Exp13_D7	25	5	625	Trisodium citrate	Na3C6H5O7	125
32	Exp13_D8	25	25	625	Trisodium citrate	Na3C6H5O7	625
33	Exp13_D9	25	125	625	Trisodium citrate	Na3C6H5O7	3125
34	Exp3_av_B1	30	30	25	Glucose	C6H12O6	900
35	Exp3_av_B2	30	30	25	Sucrose	C12H22O11	900
36	Exp3_av_B3	30	30	25	Urea	CH4N2O	900
37	Exp3_av_B4	30	30	25	Tris	C4H11NO3	900
38	Exp3_av_C2	30	30	25	Sodium acetate	C2H3NaO2	900
39	Exp3_av_C3	30	30	25	Sodium pyruvate	C3H3NaO3	900
40	Exp3_av_D1	30	30	25	Sodium formate	CHNaO2	900
41	Exp3_av_D2	30	30	25	Citric acid	C6H8O7	900
42	Exp3_low_B1	10	10	25	Glucose	C6H12O6	100
43	Exp3_low_B2	10	10	25	Sucrose	C12H22O11	100
44	Exp3_low_B3	10	10	25	Urea	CH4N2O	100
45	Exp3_low_B4	10	10	25	Tris	C4H11NO3	100
46	Exp3_low_C2	10	10	25	Sodium acetate	C2H3NaO2	100
47	Exp3_low_C4	10	10	25	Glycine	C2H5NO2	100
48	Exp3_low_D2	10	10	25	Citric acid	C6H8O7	100
49	Exp4_B1	25	25	25	Ethanol	C2H6O	625
50	Exp4_B2	25	25	25	2-propanol	C3H8O	625
51	Exp4_B3	25	25	25	Ethylene glycol	C2H6O2	625
52	Exp4_B4	25	25	25	Formamide	CH3NO	625
53	Exp4_C1	25	25	25	1-propanol	C3H8O	625
54	Exp4_C2	25	25	25	Glycol	C2H6O2	625
55	Exp4_C4	25	25	25	Sodium acetate	C2H3NaO2	625
56	Exp4_D4	25	25	1000	Glycine	C2H5NO2	625
57	Exp5_C3	25	25	25	EDTA disodium salt	C10H14N2Na2O8	625
58	Exp5_D1	25	25	25	Tricine	C6H13NO5	625
59	Exp5_D3	25	25	25	TAPS	C7H17NO6S	625
60	Exp_GLUC_B1	25	5	10	Glucose	C6H12O6	125
61	Exp_GLUC_B4	25	10	10	Glucose	C6H12O6	250
62	Exp_GLUC_B7	25	25	10	Glucose	C6H12O6	625
63	Exp_GLUC_B10	25	50	10	Glucose	C6H12O6	1250
64	Exp_GLUC_C1	25	5	25	Glucose	C6H12O6	125
65	Exp_GLUC_C4	25	10	25	Glucose	C6H12O6	250
66	Exp_GLUC_C7	25	25	25	Glucose	C6H12O6	625
67	Exp_GLUC_C10	25	50	25	Glucose	C6H12O6	1250
68	Exp_GLUC_D1	25	5	40	Glucose	C6H12O6	125
69	Exp_GLUC_D4	25	10	40	Glucose	C6H12O6	250
70	Exp_GLUC_D7	25	25	40	Glucose	C6H12O6	625
71	Exp_GLUC_D10	25	50	40	Glucose	C6H12O6	1250
72	Exp_GLUC_E1	25	5	50	Glucose	C6H12O6	125

73	Exp_GLUC_E6	25	10	50	Glucose	C6H12O6	250
74	Exp_GLUC_E8	25	25	50	Glucose	C6H12O6	625
75	Exp_GLUC_E10	25	50	50	Glucose	C6H12O6	1250
76	Exp_GLUC_F1	25	5	100	Glucose	C6H12O6	125
77	Exp_GLUC_F4	25	10	100	Glucose	C6H12O6	250
78	Exp_GLUC_F9	25	25	100	Glucose	C6H12O6	625
79	Exp_GLUC_F10	25	50	100	Glucose	C6H12O6	1250
80	Exp_GLUC_G1	25	5	125	Glucose	C6H12O6	125
81	Exp_GLUC_G4	25	10	125	Glucose	C6H12O6	250
82	Exp_GLUC_G7	25	25	125	Glucose	C6H12O6	625
83	Exp_GLUC_G10	25	50	125	Glucose	C6H12O6	1250
84	Exp_SORB_B1	25	5	10	D-Sorbitol	C6H14O6	125
85	Exp_SORB_B4	25	10	10	D-Sorbitol	C6H14O6	250
86	Exp_SORB_B7	25	25	10	D-Sorbitol	C6H14O6	625
87	Exp_SORB_B11	25	50	10	D-Sorbitol	C6H14O6	1250
88	Exp_SORB_C1	25	5	25	D-Sorbitol	C6H14O6	125
89	Exp_SORB_C4	25	10	25	D-Sorbitol	C6H14O6	250
90	Exp_SORB_C7	25	25	25	D-Sorbitol	C6H14O6	625
91	Exp_SORB_C11	25	50	25	D-Sorbitol	C6H14O6	1250
92	Exp_SORB_D1	25	5	40	D-Sorbitol	C6H14O6	125
93	Exp_SORB_D4	25	10	40	D-Sorbitol	C6H14O6	250
94	Exp_SORB_D7	25	25	40	D-Sorbitol	C6H14O6	625
95	Exp_SORB_D11	25	50	40	D-Sorbitol	C6H14O6	1250
96	Exp_SORB_E1	25	5	50	D-Sorbitol	C6H14O6	125
97	Exp_SORB_E6	25	10	50	D-Sorbitol	C6H14O6	250
98	Exp_SORB_E7	25	25	50	D-Sorbitol	C6H14O6	625
99	Exp_SORB_E11	25	50	50	D-Sorbitol	C6H14O6	1250
100	Exp_SORB_F1	25	5	100	D-Sorbitol	C6H14O6	125
101	Exp_SORB_F4	25	10	100	D-Sorbitol	C6H14O6	250
102	Exp_SORB_F7	25	25	100	D-Sorbitol	C6H14O6	625
103	Exp_SORB_F11	25	50	100	D-Sorbitol	C6H14O6	1250
104	Exp_SORB_G1	25	5	125	D-Sorbitol	C6H14O6	125
105	Exp_SORB_G4	25	10	125	D-Sorbitol	C6H14O6	250
106	Exp_SORB_G7	25	25	125	D-Sorbitol	C6H14O6	625
107	Exp_SORB_G11	25	50	125	D-Sorbitol	C6H14O6	1250
108	Exp_GLYICI_CO3_5mM_B4	5	5	10	Glycine	C2H5NO2	25
109	Exp_GLYICI_CO3_5mM_B6	5	10	10	Glycine	C2H5NO2	50
110	Exp_GLYICI_CO3_5mM_B8	5	25	10	Glycine	C2H5NO2	125
111	Exp_GLYICI_CO3_5mM_B9	5	50	10	Glycine	C2H5NO2	250
112	Exp_GLYICI_CO3_5mM_C3	5	5	20	Glycine	C2H5NO2	25
113	Exp_GLYICI_CO3_5mM_C6	5	10	20	Glycine	C2H5NO2	50
114	Exp_GLYICI_CO3_5mM_C8	5	25	20	Glycine	C2H5NO2	125
115	Exp_GLYICI_CO3_5mM_C9	5	50	20	Glycine	C2H5NO2	250
116	Exp_GLYICI_CO3_5mM_D3	5	5	25	Glycine	C2H5NO2	25
117	Exp_GLYICI_CO3_5mM_D6	5	10	25	Glycine	C2H5NO2	50
118	Exp_GLYICI_CO3_5mM_D8	5	25	25	Glycine	C2H5NO2	125
119	Exp_GLYICI_CO3_5mM_D9	5	50	25	Glycine	C2H5NO2	250
120	Exp_GLYICI_CO3_5mM_E3	5	5	50	Glycine	C2H5NO2	25
121	Exp_GLYICI_CO3_5mM_E5	5	10	50	Glycine	C2H5NO2	50
122	Exp_GLYICI_CO3_5mM_E8	5	25	50	Glycine	C2H5NO2	125
123	Exp_GLYICI_CO3_5mM_E9	5	50	50	Glycine	C2H5NO2	250
124	Exp_GLYICI_CO3_5mM_F3	5	5	100	Glycine	C2H5NO2	25
125	Exp_GLYICI_CO3_5mM_F5	5	10	100	Glycine	C2H5NO2	50
126	Exp_GLYICI_CO3_5mM_F7	5	25	100	Glycine	C2H5NO2	125

127	Exp_GLYICI_CO3_5mM_F10	5	50	100	Glycine	C2H5NO2	250
128	Exp_GLYICI_CO3_5mM_G3	5	5	500	Glycine	C2H5NO2	25
129	Exp_GLYICI_CO3_5mM_G5	5	10	500	Glycine	C2H5NO2	50
130	Exp_GLYICI_CO3_5mM_G7	5	25	500	Glycine	C2H5NO2	125
131	Exp_GLYICI_CO3_5mM_G10	5	50	500	Glycine	C2H5NO2	250
132	Exp_GLYICI_CO3_25mM_B3	25	5	10	Glycine	C2H5NO2	125
133	Exp_GLYICI_CO3_25mM_B6	25	10	10	Glycine	C2H5NO2	250
134	Exp_GLYICI_CO3_25mM_B8	25	25	10	Glycine	C2H5NO2	625
135	Exp_GLYICI_CO3_25mM_B9	25	50	10	Glycine	C2H5NO2	1250
136	Exp_GLYICI_CO3_25mM_C3	25	5	20	Glycine	C2H5NO2	125
137	Exp_GLYICI_CO3_25mM_C5	25	10	20	Glycine	C2H5NO2	250
138	Exp_GLYICI_CO3_25mM_C7	25	25	20	Glycine	C2H5NO2	625
139	Exp_GLYICI_CO3_25mM_C9	25	50	20	Glycine	C2H5NO2	1250
140	Exp_GLYICI_CO3_25mM_D3	25	5	25	Glycine	C2H5NO2	125
141	Exp_GLYICI_CO3_25mM_D6	25	10	25	Glycine	C2H5NO2	250
142	Exp_GLYICI_CO3_25mM_D7	25	25	25	Glycine	C2H5NO2	625
143	Exp_GLYICI_CO3_25mM_D9	25	50	25	Glycine	C2H5NO2	1250
144	Exp_GLYICI_CO3_25mM_E4	25	5	50	Glycine	C2H5NO2	125
145	Exp_GLYICI_CO3_25mM_E6	25	10	50	Glycine	C2H5NO2	250
146	Exp_GLYICI_CO3_25mM_E8	25	25	50	Glycine	C2H5NO2	625
147	Exp_GLYICI_CO3_25mM_E9	25	50	50	Glycine	C2H5NO2	1250
148	Exp_GLYICI_CO3_25mM_F4	25	5	100	Glycine	C2H5NO2	125
149	Exp_GLYICI_CO3_25mM_F5	25	10	100	Glycine	C2H5NO2	250
150	Exp_GLYICI_CO3_25mM_F7	25	25	100	Glycine	C2H5NO2	625
151	Exp_GLYICI_CO3_25mM_F9	25	50	100	Glycine	C2H5NO2	1250
152	Exp_GLYICI_CO3_25mM_G3	25	5	500	Glycine	C2H5NO2	125
153	Exp_GLYICI_CO3_25mM_G5	25	10	500	Glycine	C2H5NO2	250
154	Exp_GLYICI_CO3_25mM_G8	25	25	500	Glycine	C2H5NO2	625
155	Exp_GLYICI_CO3_25mM_G9	25	50	500	Glycine	C2H5NO2	1250
156	Exp_ALAN_CO3_5mM_B3	5	5	10	L-Alanine	C3H7NO2	25
157	Exp_ALAN_CO3_5mM_B6	5	10	10	L-Alanine	C3H7NO2	50
158	Exp_ALAN_CO3_5mM_B7	5	25	10	L-Alanine	C3H7NO2	125
159	Exp_ALAN_CO3_5mM_B9	5	50	10	L-Alanine	C3H7NO2	250
160	Exp_ALAN_CO3_5mM_C3	5	5	20	L-Alanine	C3H7NO2	25
161	Exp_ALAN_CO3_5mM_C5	5	10	20	L-Alanine	C3H7NO2	50
162	Exp_ALAN_CO3_5mM_C7	5	25	20	L-Alanine	C3H7NO2	125
163	Exp_ALAN_CO3_5mM_C9	5	50	20	L-Alanine	C3H7NO2	250
164	Exp_ALAN_CO3_5mM_D3	5	5	25	L-Alanine	C3H7NO2	25
165	Exp_ALAN_CO3_5mM_D5	5	10	25	L-Alanine	C3H7NO2	50
166	Exp_ALAN_CO3_5mM_D7	5	25	25	L-Alanine	C3H7NO2	125
167	Exp_ALAN_CO3_5mM_D9	5	50	25	L-Alanine	C3H7NO2	250
168	Exp_ALAN_CO3_5mM_E3	5	5	50	L-Alanine	C3H7NO2	25
169	Exp_ALAN_CO3_5mM_E5	5	10	50	L-Alanine	C3H7NO2	50
170	Exp_ALAN_CO3_5mM_E7	5	25	50	L-Alanine	C3H7NO2	125
171	Exp_ALAN_CO3_5mM_E9	5	50	50	L-Alanine	C3H7NO2	250
172	Exp_ALAN_CO3_5mM_F3	5	5	100	L-Alanine	C3H7NO2	25
173	Exp_ALAN_CO3_5mM_F5	5	10	100	L-Alanine	C3H7NO2	50
174	Exp_ALAN_CO3_5mM_F7	5	25	100	L-Alanine	C3H7NO2	125
175	Exp_ALAN_CO3_5mM_F10	5	50	100	L-Alanine	C3H7NO2	250
176	Exp_ALAN_CO3_5mM_G4	5	5	500	L-Alanine	C3H7NO2	25
177	Exp_ALAN_CO3_5mM_G5	5	10	500	L-Alanine	C3H7NO2	50
178	Exp_ALAN_CO3_5mM_G7	5	25	500	L-Alanine	C3H7NO2	125
179	Exp_ALAN_CO3_5mM_G9	5	50	500	L-Alanine	C3H7NO2	250
180	Exp_ALAN_CO3_25mM_B3	25	5	10	L-Alanine	C3H7NO2	125

181	Exp_ALAN_CO3_25mM_B5	25	10	10	L-Alanine	C3H7NO2	250
182	Exp_ALAN_CO3_25mM_B7	25	25	10	L-Alanine	C3H7NO2	625
183	Exp_ALAN_CO3_25mM_B9	25	50	10	L-Alanine	C3H7NO2	1250
184	Exp_ALAN_CO3_25mM_C3	25	5	20	L-Alanine	C3H7NO2	125
185	Exp_ALAN_CO3_25mM_C5	25	10	20	L-Alanine	C3H7NO2	250
186	Exp_ALAN_CO3_25mM_C7	25	25	20	L-Alanine	C3H7NO2	625
187	Exp_ALAN_CO3_25mM_C9	25	50	20	L-Alanine	C3H7NO2	1250
188	Exp_ALAN_CO3_25mM_D3	25	5	25	L-Alanine	C3H7NO2	125
189	Exp_ALAN_CO3_25mM_D5	25	10	25	L-Alanine	C3H7NO2	250
190	Exp_ALAN_CO3_25mM_D7	25	25	25	L-Alanine	C3H7NO2	625
191	Exp_ALAN_CO3_25mM_D9	25	50	25	L-Alanine	C3H7NO2	1250
192	Exp_ALAN_CO3_25mM_E3	25	5	50	L-Alanine	C3H7NO2	125
193	Exp_ALAN_CO3_25mM_E5	25	10	50	L-Alanine	C3H7NO2	250
194	Exp_ALAN_CO3_25mM_E7	25	25	50	L-Alanine	C3H7NO2	625
195	Exp_ALAN_CO3_25mM_E9	25	50	50	L-Alanine	C3H7NO2	1250
196	Exp_ALAN_CO3_25mM_F3	25	5	100	L-Alanine	C3H7NO2	125
197	Exp_ALAN_CO3_25mM_F5	25	10	100	L-Alanine	C3H7NO2	250
198	Exp_ALAN_CO3_25mM_F7	25	25	100	L-Alanine	C3H7NO2	625
199	Exp_ALAN_CO3_25mM_F9	25	50	100	L-Alanine	C3H7NO2	1250
200	Exp_ALAN_CO3_25mM_G3	25	5	500	L-Alanine	C3H7NO2	125
201	Exp_ALAN_CO3_25mM_G5	25	10	500	L-Alanine	C3H7NO2	250
202	Exp_ALAN_CO3_25mM_G7	25	25	500	L-Alanine	C3H7NO2	625
203	Exp_ALAN_CO3_25mM_G10	25	50	500	L-Alanine	C3H7NO2	1250
204	BASELINE_D3	5	5	0	No additive	H2O	25
205	BASELINE_D6	5	10	0	No additive	H2O	50
206	BASELINE_D7	5	25	0	No additive	H2O	125
207	BASELINE_D9	5	50	0	No additive	H2O	250
208	BASELINE_E3	25	5	0	No additive	H2O	125
209	BASELINE_E5	25	10	0	No additive	H2O	250
210	BASELINE_E8	25	25	0	No additive	H2O	625
211	BASELINE_E9	25	50	0	No additive	H2O	1250
212	Exp_SUCR_CO3_5mM_B3	5	5	10	Sucrose	C12H22O11	25
213	Exp_SUCR_CO3_5mM_B5	5	10	10	Sucrose	C12H22O11	50
214	Exp_SUCR_CO3_5mM_B7	5	25	10	Sucrose	C12H22O11	125
215	Exp_SUCR_CO3_5mM_B9	5	50	10	Sucrose	C12H22O11	250
216	Exp_SUCR_CO3_5mM_C3	5	5	20	Sucrose	C12H22O11	25
217	Exp_SUCR_CO3_5mM_C5	5	10	20	Sucrose	C12H22O11	50
218	Exp_SUCR_CO3_5mM_C7	5	25	20	Sucrose	C12H22O11	125
219	Exp_SUCR_CO3_5mM_C10	5	50	20	Sucrose	C12H22O11	250
220	Exp_SUCR_CO3_5mM_D3	5	5	25	Sucrose	C12H22O11	25
221	Exp_SUCR_CO3_5mM_D5	5	10	25	Sucrose	C12H22O11	50
222	Exp_SUCR_CO3_5mM_D8	5	25	25	Sucrose	C12H22O11	125
223	Exp_SUCR_CO3_5mM_D10	5	50	25	Sucrose	C12H22O11	250
224	Exp_SUCR_CO3_5mM_E3	5	5	50	Sucrose	C12H22O11	25
225	Exp_SUCR_CO3_5mM_E5	5	10	50	Sucrose	C12H22O11	50
226	Exp_SUCR_CO3_5mM_E7	5	25	50	Sucrose	C12H22O11	125
227	Exp_SUCR_CO3_5mM_E9	5	50	50	Sucrose	C12H22O11	250

228	Exp_SUCR_CO3_5mM_F3	5	5	100	Sucrose	C12H22O11	25
229	Exp_SUCR_CO3_5mM_F5	5	10	100	Sucrose	C12H22O11	50
230	Exp_SUCR_CO3_5mM_F7	5	25	100	Sucrose	C12H22O11	125
231	Exp_SUCR_CO3_5mM_F9	5	50	100	Sucrose	C12H22O11	250
232	Exp_SUCR_CO3_5mM_G3	5	5	500	Sucrose	C12H22O11	25
233	Exp_SUCR_CO3_5mM_G5	5	10	500	Sucrose	C12H22O11	50
234	Exp_SUCR_CO3_5mM_G7	5	25	500	Sucrose	C12H22O11	125
235	Exp_SUCR_CO3_5mM_G9	5	50	500	Sucrose	C12H22O11	250
236	Exp_URE_CO3_5mM_B3	5	5	10	Urea	CH4N2O	25
237	Exp_URE_CO3_5mM_B5	5	10	10	Urea	CH4N2O	50
238	Exp_URE_CO3_5mM_B7	5	25	10	Urea	CH4N2O	125
239	Exp_URE_CO3_5mM_B9	5	50	10	Urea	CH4N2O	250
240	Exp_URE_CO3_5mM_C3	5	5	20	Urea	CH4N2O	25
241	Exp_URE_CO3_5mM_C5	5	10	20	Urea	CH4N2O	50
242	Exp_URE_CO3_5mM_C7	5	25	20	Urea	CH4N2O	125
243	Exp_URE_CO3_5mM_C9	5	50	20	Urea	CH4N2O	250
244	Exp_URE_CO3_5mM_D3	5	5	25	Urea	CH4N2O	25
245	Exp_URE_CO3_5mM_D5	5	10	25	Urea	CH4N2O	50
246	Exp_URE_CO3_5mM_D7	5	25	25	Urea	CH4N2O	125
247	Exp_URE_CO3_5mM_D9	5	50	25	Urea	CH4N2O	250
248	Exp_URE_CO3_5mM_E3	5	5	50	Urea	CH4N2O	25
249	Exp_URE_CO3_5mM_E5	5	10	50	Urea	CH4N2O	50
250	Exp_URE_CO3_5mM_E7	5	25	50	Urea	CH4N2O	125
251	Exp_URE_CO3_5mM_E9	5	50	50	Urea	CH4N2O	250
252	Exp_URE_CO3_5mM_F4	5	5	100	Urea	CH4N2O	25
253	Exp_URE_CO3_5mM_F5	5	10	100	Urea	CH4N2O	50
254	Exp_URE_CO3_5mM_F7	5	25	100	Urea	CH4N2O	125
255	Exp_URE_CO3_5mM_F9	5	50	100	Urea	CH4N2O	250
256	Exp_URE_CO3_5mM_G3	5	5	500	Urea	CH4N2O	25
257	Exp_URE_CO3_5mM_G5	5	10	500	Urea	CH4N2O	50
258	Exp_URE_CO3_5mM_G7	5	25	500	Urea	CH4N2O	125
259	Exp_URE_CO3_5mM_G9	5	50	500	Urea	CH4N2O	250
260	Exp_URE_CO3_25mM_B3	25	5	10	Urea	CH4N2O	125
261	Exp_URE_CO3_25mM_B5	25	10	10	Urea	CH4N2O	250
262	Exp_URE_CO3_25mM_B7	25	25	10	Urea	CH4N2O	625
263	Exp_URE_CO3_25mM_B9	25	50	10	Urea	CH4N2O	1250
264	Exp_URE_CO3_25mM_C3	25	5	20	Urea	CH4N2O	125
265	Exp_URE_CO3_25mM_C5	25	10	20	Urea	CH4N2O	250
266	Exp_URE_CO3_25mM_C7	25	25	20	Urea	CH4N2O	625
267	Exp_URE_CO3_25mM_C9	25	50	20	Urea	CH4N2O	1250
268	Exp_URE_CO3_25mM_D3	25	5	25	Urea	CH4N2O	125
269	Exp_URE_CO3_25mM_D5	25	10	25	Urea	CH4N2O	250
270	Exp_URE_CO3_25mM_D7	25	25	25	Urea	CH4N2O	625
271	Exp_URE_CO3_25mM_D9	25	50	25	Urea	CH4N2O	1250
272	Exp_URE_CO3_25mM_E3	25	5	50	Urea	CH4N2O	125
273	Exp_URE_CO3_25mM_E5	25	10	50	Urea	CH4N2O	250
274	Exp_URE_CO3_25mM_E7	25	25	50	Urea	CH4N2O	625
275	Exp_URE_CO3_25mM_E9	25	50	50	Urea	CH4N2O	1250
276	Exp_URE_CO3_25mM_F3	25	5	100	Urea	CH4N2O	125
277	Exp_URE_CO3_25mM_F5	25	10	100	Urea	CH4N2O	250
278	Exp_URE_CO3_25mM_F7	25	25	100	Urea	CH4N2O	625
279	Exp_URE_CO3_25mM_F9	25	50	100	Urea	CH4N2O	1250
280	Exp_URE_CO3_25mM_G3	25	5	500	Urea	CH4N2O	125
281	Exp_URE_CO3_25mM_G5	25	10	500	Urea	CH4N2O	250

282	Exp_URE_CO3_25mM_G7	25	25	500	Urea	CH4N2O	625
283	Exp_URE_CO3_25mM_G9	25	50	500	Urea	CH4N2O	1250
284	Exp_SUCR_CO3_25mM_B3	25	5	10	Sucrose	C12H22O11	125
285	Exp_SUCR_CO3_25mM_B5	25	10	10	Sucrose	C12H22O11	250
286	Exp_SUCR_CO3_25mM_B7	25	25	10	Sucrose	C12H22O11	625
287	Exp_SUCR_CO3_25mM_B9	25	50	10	Sucrose	C12H22O11	1250
288	Exp_SUCR_CO3_25mM_C3	25	5	20	Sucrose	C12H22O11	125
289	Exp_SUCR_CO3_25mM_C5	25	10	20	Sucrose	C12H22O11	250
290	Exp_SUCR_CO3_25mM_C7	25	25	20	Sucrose	C12H22O11	625
291	Exp_SUCR_CO3_25mM_C9	25	50	20	Sucrose	C12H22O11	1250
292	Exp_SUCR_CO3_25mM_D3	25	5	25	Sucrose	C12H22O11	125
293	Exp_SUCR_CO3_25mM_D5	25	10	25	Sucrose	C12H22O11	250
294	Exp_SUCR_CO3_25mM_D8	25	25	25	Sucrose	C12H22O11	625
295	Exp_SUCR_CO3_25mM_D10	25	50	25	Sucrose	C12H22O11	1250
296	Exp_SUCR_CO3_25mM_E4	25	5	50	Sucrose	C12H22O11	125
297	Exp_SUCR_CO3_25mM_E5	25	10	50	Sucrose	C12H22O11	250
298	Exp_SUCR_CO3_25mM_E7	25	25	50	Sucrose	C12H22O11	625
299	Exp_SUCR_CO3_25mM_E9	25	50	50	Sucrose	C12H22O11	1250
300	Exp_SUCR_CO3_25mM_F3	25	5	100	Sucrose	C12H22O11	125
301	Exp_SUCR_CO3_25mM_F5	25	10	100	Sucrose	C12H22O11	250
302	Exp_SUCR_CO3_25mM_F7	25	25	100	Sucrose	C12H22O11	625
303	Exp_SUCR_CO3_25mM_F9	25	50	100	Sucrose	C12H22O11	1250
304	Exp_SUCR_CO3_25mM_G4	25	5	500	Sucrose	C12H22O11	125
305	Exp_SUCR_CO3_25mM_G5	25	10	500	Sucrose	C12H22O11	250
306	Exp_SUCR_CO3_25mM_G7	25	25	500	Sucrose	C12H22O11	625
307	Exp_SUCR_CO3_25mM_G9	25	50	500	Sucrose	C12H22O11	1250

Table S1. Overview of the 307 calcium carbonate mineralization experiments analyzed in this study. For each experiment, the table reports the experimental ID, Na_2CO_3 concentration, $CaCl_2{\cdot}2H_2O$ concentration, organic additive concentration, organic additive identity and formula, and the ionic activity product (IAP = $[Na_2CO_3] \times [CaCl_2{\cdot}2H_2O]$). The dataset includes additive-free baseline conditions and organics-mediated experiments performed with 23 organic additives across varied solution compositions.

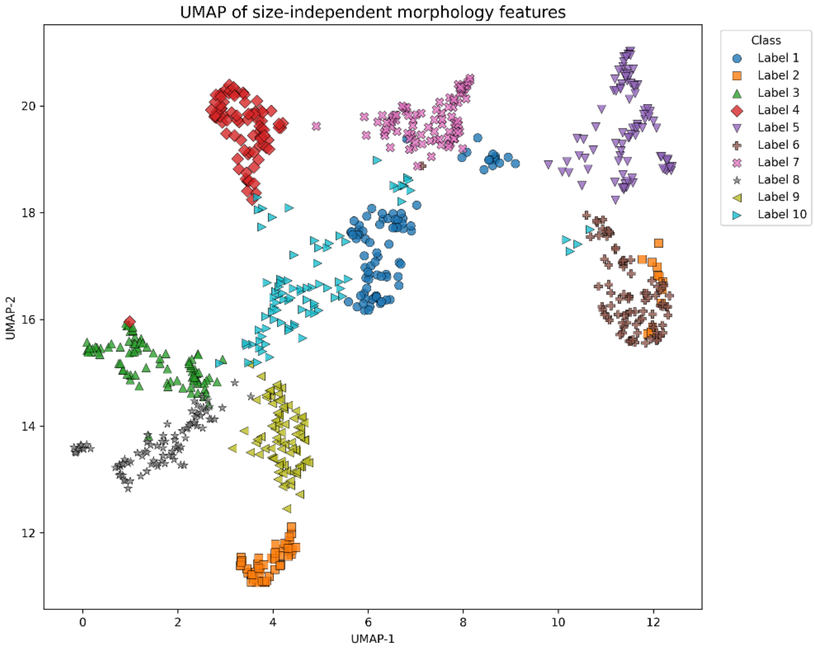

Figure S1. UMAP embedding of particles based on size-independent morphological and texture descriptors. Points are colored according to the ten morphological particle types (P1–P10) identified from microscopy. Distinct clusters indicate that the morphotypes correspond to separable regions in feature space.

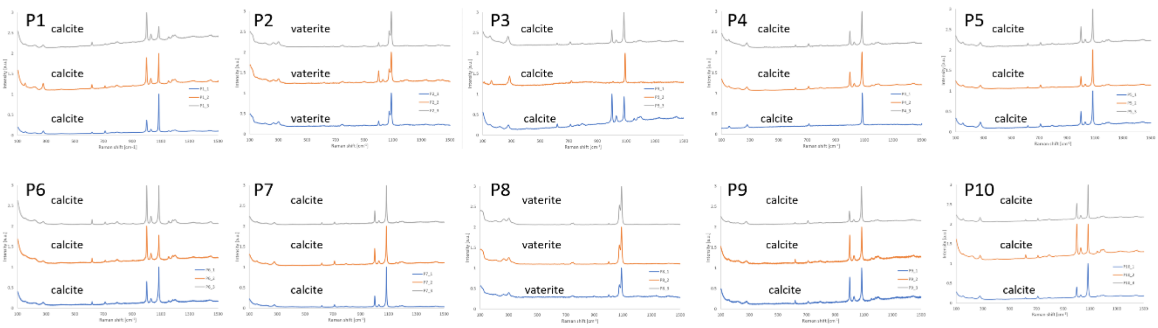

Figure S2. Raman spectroscopic identification of mineral phases associated with the ten $CaCO_3$ particle morphotypes identified in the main text (P1–P10). Raman spectra of representative particles belonging to each morphotype are shown (three examples displayed per morphotype, P*_1–P*_3); in total, >30 particles per morphotype were analyzed. Morphotypes P1, P3–P7, P9, and P10 exhibit characteristic calcite Raman bands, including lattice modes at ~156 and ~282 cm^{-1}, the in-plane bending mode (ν_4) at ~712 cm^{-1}, and a dominant symmetric carbonate stretching mode (ν_1) at ~1086 cm^{-1}. Morphotypes P2 and P8 display Raman features characteristic of vaterite, including the splitting of the ν_1 symmetric stretching mode forming a triplet in the ~1074–1091 cm^{-1} region, lattice modes around ~266–301 cm^{-1}, and multiple bands in the ν_4 in-plane bending region (~650–780 cm^{-1}). Additional peaks attributable to polystyrene from the well plate substrate are occasionally observed, most prominently the aromatic ring breathing mode at ~1001 cm^{-1}, together with other characteristic bands in the ~620–620 cm^{-1} and ~1030–1600 cm^{-1} regions.

S1. Validation of plate surface treatment

To validate the use of plasma-treated tissue-culture plates in the high-throughput mineralization experiments, control assays were conducted using untreated glass plates under identical solution chemistry. These tests confirmed that the surface treatment enhanced particle adhesion to the well bottom without altering the mineral morphology or composition. Results are shown in Figure S3.

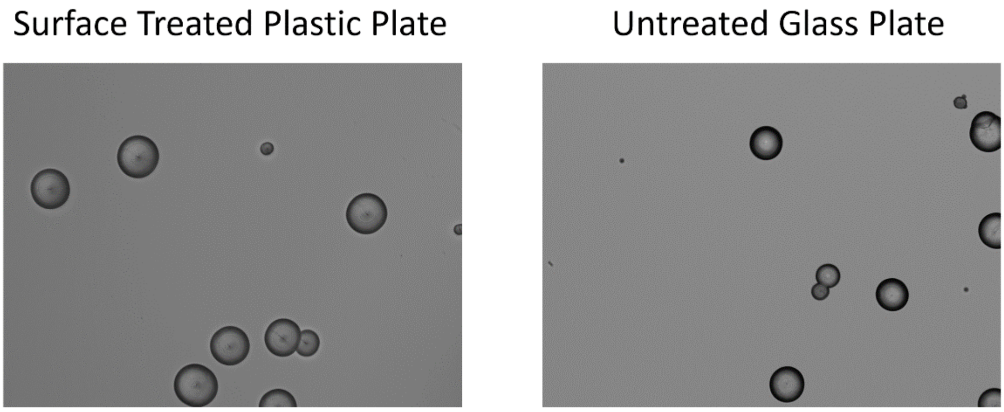

Figure S3. Comparison between surface-treated plastic and untreated glass plates used for mineralization experiments. Representative optical images (field of view: 1024 µm × 781.5 µm) showing calcium carbonate particles formed in the presence of Na-acetate on (left) a plasma-treated polystyrene plate and (right) an untreated glass plate. The surface-treated plates promoted particle adhesion to the well bottom, minimizing drift during imaging and enabling stable *in-situ* analysis. In both cases, spherical particles of comparable size were observed, and Raman spectroscopy confirmed that all were composed of calcite.

S2. Particle detection and morphological characterization pipeline

This section provides the full methodological detail of the image-analysis workflow described in Section 4.3 of the main text. It includes a step-by-step description of particle detection, feature extraction, and computation of both primary and derived descriptors.

S2.1 Detailed detection and feature extraction workflow

Stitched well images (TIFF) were processed with a custom Python/OpenCV pipeline to detect individual particles, assign a unique Particle Index, and compute a comprehensive set of geometric and texture descriptors. Each well image was converted to binary by global intensity thresholding (binary-inverse), and external contours were extracted using OpenCV's `findContours`. Contours intersecting the circular field-of-view boundary (within a 3-pixel margin) were excluded to avoid truncated particles. Objects smaller or larger than the user-defined area range (typically 100–500,000 px) were removed. The remaining contours were processed one-by-one to compute full-resolution geometric and intensity-based features.

S2.1.1 Geometric and size descriptors

For each contour, the following parameters were extracted: area, perimeter, equivalent diameter, bounding-box width and height, best-fit ellipse major/minor axes (where applicable), aspect ratio, eccentricity, elongation, circularity, solidity, extent, rectangularity, and convexity (hull perimeter/perimeter). Additional descriptors included skeleton length, radius of gyration, equivalent rectangular aspect ratio, radial peak count (local maxima in the radial distance profile from the centroid), fractal dimension (box-count method), and convexity defect metrics (mean depth, maximum depth, and count). Fourier shape descriptors (magnitudes of the first 10 DFT coefficients) and invariant spatial moments (μ_{pq}) and Hu moments (1–7) were also calculated.

S2.1.2 Optical intensity and texture descriptors

For each detected particle, an adaptive down-scaled region of interest (ROI) was generated to compute texture descriptors efficiently. Intensity statistics (mean, standard deviation, median, min, max, P10, P90, inter-percentile range) were derived from the masked ROI. Rim-versus-core and local background metrics were computed by morphological erosion and dilation to define the rim, core, and background regions. Corresponding mean intensities and ratios (e.g., rim/core and particle/background) were recorded. Textural descriptors were extracted from grey-level co-occurrence matrices (GLCM) at 0° and 90° (contrast, homogeneity, correlation, ASM) and from local binary patterns (LBP, P=8, R=2). Edge-based metrics included the mean gradient magnitude and the variance of the Laplacian to capture fine-scale surface detail.

All particles were indexed sequentially and stored alongside their descriptors. For each well, the pipeline exported (i) a CSV file containing all descriptors per particle, and (ii) an overlay image showing detected contours and indices.

S2.1.3 Derived parameters for downstream analysis

Starting from the primary descriptors, a second processing stage was applied to compute a series of derived morphological and statistical parameters. These additional descriptors were designed to capture inter-feature relationships and enhance the discrimination between particle types. The derived parameters included normalized and ratio-based metrics such as the area-to-perimeter ratio, elongation-to-circularity ratio, and solidity-weighted eccentricity, which reduce the influence of particle size while improving sensitivity to shape variations.

Composite roughness indices were also calculated by combining measures such as fractal dimension, convexity defects, and Fourier harmonic amplitudes, providing a quantitative estimate of boundary irregularity and surface faceting. To characterize overall form balance, symmetry and anisotropy descriptors were derived from moment invariants and aspect ratios, enabling the distinction between isotropic particles and those exhibiting directional elongation or lobed morphologies.

In addition, aggregate statistical parameters—including z-scored, log-transformed, and variance-normalized variables—were computed to facilitate cross-comparison among wells and experimental plates. Texture contrast indices were obtained by combining grey-level co-occurrence matrix (GLCM) and local binary pattern (LBP) outputs, allowing simultaneous characterization of both coarse and fine-scale optical heterogeneity within each particle.

Finally, feature correlation metrics were generated to describe multivariate relationships among morphological and textural variables, such as the correlation between area, circularity, and texture contrast, which highlight systematic patterns of particle differentiation.

These derived descriptors provide complementary information to the primary measurements, ensuring that subtle differences in particle roughness, symmetry, and internal optical texture are quantitatively represented. Together, the primary and derived feature sets form the complete dataset used for downstream machine-learning–based particle classification and targeted Raman phase assignment described below.

S2.2 Morphological and textural parameters

The following sub-sections provide the complete list and definitions of all morphological and textural descriptors calculated by the image-analysis pipeline described in Section 4.3 of the main text. These parameters include both primary descriptors (directly extracted from optical images) and derived descriptors (computed from the primary set through normalization, ratios, or multivariate relationships). Together, they represent the full quantitative feature space used for subsequent statistical and machine-learning analyses.

S2.2.1 Primary descriptors

All parameters calculated from optical images are listed below and can be classified into the following descriptor groups. Each group captures a different aspect of particle morphology or optical texture, providing complementary quantitative information used for subsequent statistical and machine-learning analyses. Column names in the exported *.csv* file are indicated in *italics*.

A. Size & basic geometry (scale-dependent size and footprint)

- *Area*, *Perimeter*, *Equivalent Diameter*, *Bounding Box Width/Height*. Quantify particle size and footprint; useful for growth/kinetics and for separating small seeds from larger aggregates.

B. Ellipse-based shape & compactness (gross morphology)

- *Major Axis Length*, *Minor Axis Length*, *Aspect Ratio*, *Eccentricity*, *Elongation*, *Circularity*, *Solidity*, *Extent*, *Rectangularity*, *Convexity*. Capture deviations from equant shapes (e.g., needles/plates vs equant crystals), packing/aggregation, and surface faceting.

C. Skeleton/structure & radial geometry (branching and radial order)

- *Skeleton Length* (1-px skeleton length), *Radius of Gyration*, *Equivalent Rectangular Aspect Ratio*, *Radial Peak Count*. Probe internal branching/aggregation (skeleton), characteristic size (gyration), and angular/radial modulation (peaks).

D. Boundary roughness & complexity (edge-level descriptors)

- *Fractal Dimension*, *Mean Convexity Defect Depth*, *Max Convexity Defect Depth*, *Number of Convexity Defects*. Quantify boundary indents/protrusions (growth instabilities, spherulitic vs faceted habits).

E. Moments (invariant shape signatures)

- *Spatial Moments μ_{pq}* (central moments; exported as *Spatial Moment mu…*), *Hu Moment 1–7*. Provide rotation/scale/translation-invariant descriptors; effective for class separation when shapes are similar in size.

F. Fourier boundary descriptors (periodic boundary content)

- *Fourier Mag 1–10*. Encode dominant harmonic content of the boundary—useful for distinguishing regular faceting from lobed/ruffled edges.

G. Intensity statistics (optical contrast)

- *I Mean*, *I Std*, *I Median*, *I Min*, *I Max*, *I P10*, *I P90*, *I IPR*. Capture optical density variation (e.g., birefringence/phase contrast differences, internal occlusion).

H. Rim–core and local-background metrics (interface physics)

- *I Rim Mean*, *I Core Mean*, *I Rim-Core Δ*, *I Rim/Core Ratio*; *I-LocalBG Δ*, *I-LocalBG Z*. Highlight edge-brightening/darkening (rim growth, hollowing) and contrast relative to immediate background.

I. GLCM texture (short-range texture; 8 levels; 0°, 90°)

- *GLCM Contrast*, *GLCM Homogeneity*, *GLCM Correlation*, *GLCM ASM*. Characterize granularity and local order; sensitive to polycrystalline vs single-crystal interiors and surface texture.

J. LBP (micro-texture; P=8, R=2, uniform)

- *LBP U0 … LBP U10*. Robust to illumination shifts; captures micro-patterns indicative of spherulites, radial fibers, or faceted interiors.

K. Gradient/Laplacian (edge energy and sharpness)

- *Grad Mean* (Sobel magnitude mean), *Laplacian Var* (variance). Summaries overall edge energy and fine-scale sharpness; helpful for differentiating smooth vs highly edged particles.

S2.2 Derived descriptors

After the initial feature extraction, each per-well CSV was processed through an auxiliary Python module to compute additional derived descriptors. These parameters expand on the primary features by incorporating normalization, ratios, and multivariate relationships, providing greater sensitivity for classification.

A. Normalized ratios and dimensionless metrics

- *Area/Perimeter Ratio*, *Elongation/Circularity*, *Solidity/Eccentricity*, *Equivalent Diameter/Radius of Gyration.* Dimensionless measures that correct for particle size and yield scale-independent shape information.

B. Composite roughness and boundary irregularity

- *Roughness Index 1* = weighted combination of (1–Solidity), Fractal Dimension deviation, and Mean Convexity Defect Depth.
- *Roughness Index 2* = sum of Fourier Mag (2–5) normalized by total perimeter. These capture both small-scale protrusions and periodic boundary modulations.

C. Symmetry and anisotropy descriptors

- *Moment Symmetry Index* (ratio of Hu Moments 1/2 to total Hu moment sum).
- *Anisotropy Factor* (Major/Minor Axis ratio × Eccentricity). Quantify geometric balance and directional bias.

D. Statistical normalization and transformations

- *Z-score normalization* for all continuous variables within each plate to remove inter-plate intensity variability.
- *Log-transformed area* and *log-perimeter* to linearize growth-scaling relationships.

E. Texture composite indices

- *GLCM-LBP Fusion Contrast* = weighted mean of GLCM Contrast and LBP variance.
- *Texture Uniformity Index* = 1 – normalized variance of LBP histogram. Capture intra-particle heterogeneity that reflects polycrystallinity or internal zoning.

F. Feature correlation and multivariate relations

- *Shape–Texture Correlation* (Pearson r between Circularity and GLCM Homogeneity).
- *Size–Roughness Correlation* (r between Area and Roughness Index 1). These describe how morphology co-varies with texture, helping identify systematic patterns among growth regimes.

S3. Machine learning–based classification of distinct particle types

This section provides the full methodological detail of the machine learning workflow described in Section 4.4 of the main text. It outlines the Random Forest (RF) classification framework used to distinguish morphologically distinct particle types, including feature selection, model training, optimization, validation, and application to unseen experimental datasets.

S3.1 Model architecture and training protocol

Classification is performed using a Random Forest (RF) model implemented in *scikit-learn* (Python). Each model consists of 100 decision trees, trained using the Gini impurity criterion and random feature sampling at each split (*max_features* = $\sqrt{n}$). The ensemble approach reduces variance and captures non-linear relationships between descriptors.

Model training uses manually labelled datasets, in which representative particles are visually assigned to predefined morphological categories based on optical inspection. The numerical descriptors corresponding to each labelled particle are extracted from the master dataset. To mitigate class imbalance, an equal number of particles per class are selected by random sampling.

S3.2 Feature space and selection

The complete set of primary and derived descriptors generated by the image-analysis pipeline (Sections S2.1–S2.2) is screened prior to model training. Highly correlated features ($|r| > 0.95$) are removed to reduce redundancy, and alternative feature subsets are tested systematically to identify combinations that yield the highest classification accuracy. This procedure ensures that only the most informative and independent descriptors are retained for final model training.

S3.3 Model optimization and validation

Model performance is evaluated using five-fold cross-validation, in which the dataset is randomly divided into five equal parts. Four folds are used for training and one for validation in each iteration, ensuring every subset contributes to both stages. The mean cross-validation accuracy serves as the principal performance metric.

Predictions obtained from the validation folds are used to compute a confusion matrix, which visualizes the correspondence between true and predicted morphological classes. The matrix reveals which particle types are most frequently misclassified as one another and thus provides a qualitative measure of class separability. These insights guide iterative refinement of the feature set or morphological class definitions.

S3.4 Feature importance

Feature-importance values (scikit-learn attribute *feature_importances_*) quantify the relative contribution of each descriptor to class discrimination. Ranking these values highlights the most influential geometric and textural features, enabling targeted optimization of the descriptor set for future model iterations.

S3.5 Application to unseen datasets and probability thresholding

After validation, the trained Random Forest classifier is applied to unseen experimental datasets. For each particle, the model outputs a predicted morphological type and a classification probability, corresponding to the fraction of trees in the ensemble that vote for that class.

A confidence threshold (typically ≥ 0.7) is applied so that only high-confidence assignments are retained. Particles falling below the threshold are labelled as *unclassified*. Examination of these unclassified particles enables the detection of previously unrepresented morphologies, particularly when applying the model to experiments conducted under new physicochemical conditions.